Progress in Organic Coatings 174 (2023) 107323

Contents lists available at ScienceDirect

Progress in Organic Coatings

journal homepage: www.elsevier.com/locate/porgcoat

Hairy superhydrophobic surfaces with excellent mechanical robustness, underwater stability and drag-reduction property

Liangpei Zhang [a,b], Zhaohui Huang [b,*], Wenfu Cai [a], Xiao Xue [a], Xin Min [b], Hui Zhang [a,*], Zhong Zhang [a,*]

[a] CAS Key Laboratory of Nanosystem and Hierarchical Fabrication and CAS Center for Excellence in Nanoscience, National Center for Nanoscience and Technology, Beijing 100190, China

[b] Beijing Key Laboratory of Materials Utilization of Nonmetallic Minerals and Solid Wastes, National Laboratory of Mineral Materials, School of Materials Science and Technology, China University of Geosciences, Beijing 100083, China

ARTICLE INFO

Keywords:
Superhydrophobic surface
Electrostatic flocking
Robustness
Abrasion resistance
Drag-reduction

ABSTRACT

Since superhydrophobic surfaces show extremely low friction with water, they have been tried for drag-reduction purpose for ships or pipe systems for liquid transportation in recent years. However, the superhydrophobic surfaces combining comprehensive performance, feasible fabrication method as well as low manufacturing cost are still big issues, limiting their real applications. Inspired by the fine hairs and cilia of creature, we prepare hairy surfaces by electrostatic flocking and subsequent surface modification. The optimal hairy surfaces exhibit excellent superhydrophobicity, satisfactory abrasion resistance that is superior to the superhydrophobic surfaces ever reported, long-term underwater stability with/without additional air pressure and good drag-reduction efficiency at low shearing rates. The correlations between microstructure of samples and key properties are analyzed. This work may shed new light on design and preparation of mechanical robust, underwater stable and drag-reduction surfaces that can be easily manufactured in large scale.

1. Introduction

More than 90 % of the country's trade is realized by shipping, which consumes hundreds of million tons of fossil fuel in one year [1]. Developing of drag-reduction surface is very necessary for ships to reduce the fuel consumption. In recent decades various drag-reduction surfaces have been developed, such as riblet [2–6], flexible wall [7], air bubble [8–10], superhydrophobic surface (SHS) [11–18]. Among them, the SHS, owing to its superior drag-reduction level at lower rate of water flow, has attracted significant interest for researchers. The drag-reduction mechanism of SHS originates from its unique nano- and micro-structures containing a large amount of air, which can reduce liquid-solid contact area and thus decreasing friction between water and the surface effectively [16,19,20]. However, the fine microstructures of SHS are fragile and easily damaged when subjected to water repeated washing; in addition, maintaining the long-term stability of air layer under water is also big challenge [21,22].

In nature after a long time of evolution some creatures have developed superhydrophobic surfaces featuring superior mechanical robustness and long-term stability under water. The excellent performance of these surfaces is probably due to the hairy building blocks with high aspect ratio. For example, with superhydrophobic fluffy legs, the water walking arthropods can float and move quickly on water [23–27] (Fig. 1a-b). Salvinia develops elastic eggbeater-shaped hairs on its surface, by which it has excellent long-term air-retention properties [28–30](Fig. 1c-d). Some waterfowls (e. g. ducks [31], penguins [32] …) grow superhydrophobic and drag-reduction feathers, also. Mimicing Salvinia surface, Xiang [33] et al. fabricated 3D-printed artificial hair-like structures, with which the continuous air mattress can recover completely after collapse due to various disturbances. Maryna [21] prepared the nanofur surface by hot pulling method and realized fairly stable gas layer and obvious drag-reduction effect using this surface.

In this study, the hairy surfaces were fabricated by combining the electrostatic flocking and surface modification technique using low surface energy polydimethylsiloxane (PDMS) and hydrophobic silica nanoparticles. The samples had excellent superhydrophobic performance, good abrasion resistance, and showed long-term stability of gas layer as well as superior drag-reduction effect when immersed under

* Corresponding authors.
E-mail addresses: liangpeizhang@pku.edu.cn (L. Zhang), huang118@cugb.edu.cn (Z. Huang), zhangh@nanoctr.cn (H. Zhang), zhong.zhang@nanoctr.cn (Z. Zhang).

https://doi.org/10.1016/j.porgcoat.2022.107323
Received 7 September 2022; Received in revised form 4 November 2022; Accepted 12 November 2022
Available online 18 November 2022

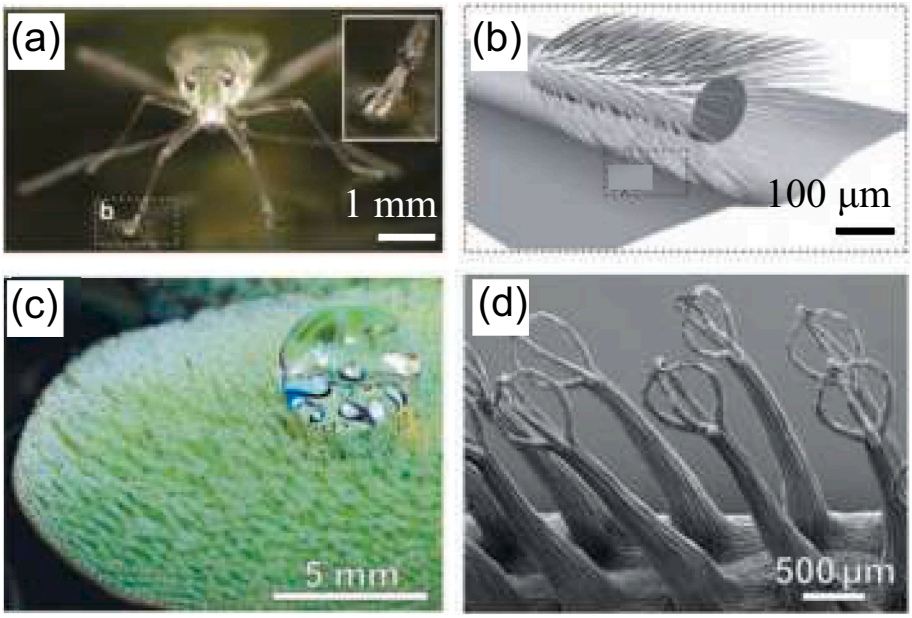

Fig. 1. Hairy superhydrophobic surfaces in nature. (a) A photo of water walking arthropod (Mesovelia) [34] floating on water and (b) related schematic microstructure of its hairy leg. (c) superhydrophobic upper side of Salvinia leaf and (d) related SEM image showing eggbeater-shaped hairy microstructure [28].

Table 1
Information of the nylon flocks and flocking density of samples.

Nominal fiber length (mm)	0.3	0.6	0.8	1.0	1.5	3.0
Av. fiber length (μm)	287 ± 48	585 ± 22	824 ± 25	998 ± 76	1485 ± 46	2985 ± 107
Av. fiber diameter (μm)	12.6	12.6	12.6	12.6	24.9	36.2
Flocking density (fiber/mm^2)	967	650	386	278	119	116

water. This hairy surface may find possible applications in drag-reduction field.

2. Experimental

2.1. Materials

Different nylon flocks with the nominal fiber length from 0.3 to 3 mm (Table 1) were provided by Alpha Flock Ltd., China. Its melting temperature was 211 °C. Isopropanol, glycerol, petroleum ether with the boiling range 60–90 °C were purchased from Sinpharm Chemical Reagent Beijing Co., Ltd., China. Polydimethylsiloxane (PDMS, Sylgard 184) was provided by Dow Corning, USA. Fumed nano-SiO_2 R812s was supplied by Evonik Industries AG, Germany. Epoxy resin, E51, was purchased from China Petrochemical Corporation, China. The curing agent was the mixture of methyl hexahydrophthalic anhydride and *N*, *N*-dimethyl benzyl amine at a mass ratio of 100:1, which were supplied by Shanghai Macklin Biochemical Technology Co., Ltd. China.

2.2. Fabrication of flocking samples

The epoxy resin E51, curing agent and nano-SiO_2 R812s (as thixotropic agent) were mechanically stirred and degassed at a mass ratio of 100:93:1.5 using Planetary Centrifugal Mixer (THINKY ARV-310LED, Thinky Corporation, Japan) for 4 min. The resulting mixture was used as the flocking adhesive in the following step.

A self-made electrostatic flocking box was used for fabrication of the flocking samples. Fig. S1 illustrates the general principle of the flocking process. The high-voltage DC power (HVDC) having the maximum voltage up to 130 kV was supplied by Spellman High Voltage Electronics CO., LTD (SL300, USA). Two parallel steel plates (20 cm × 20 cm) with a spacing of 5 cm were used as the electrodes. The upper plate was grounded and the lower plate was connected with the HVDC positive pole. Before flocking, a certain amount of nylon flocks with various nominal fiber length was evenly scattered on the lower plate with a vibrating screen. An aluminum foil, which was coated with the uncured epoxy flocking adhesive by a 50 μm wire rod coater (OSP wire rod coater), was fixed facedown under the upper plate. During flocking, the voltage 26 kV was loaded between plates. The flocking fibers were found to nearly vertically insert into the adhesive on the upper plate in the flocking time of 10 s. The sample was subsequently cured in an oven at 100 °C for 12 h. The floating flocks were blown off with a high-pressure air gun at 0.5 MPa. Six types of nylon flocks were used and their dimension parameter and the flocking density of the samples were shown in Table 1.

The flocking samples were cleaned with isopropanol twice, dried and subsequently immersed in 1 wt% PDMS-petroleum ether solution (labelled as Flock@PDMS) or 1 wt% PDMS-1 wt% nano-SiO_2 (R812s)-petroleum ether solution (Flock@PDMS-SiO_2) for 1 min for surface modification. The wetted samples were hung upside down for drying, and then put into an oven of 60 °C for 12 h. After curing, the superhydrophobic flocking samples were obtained.

2.3. Characterization

2.3.1. Surface morphology and composition

The surface morphologies of flocking samples were examined using a field emission scanning electron microscope (SEM SU8200, Hitachi, Japan) at an accelerating voltage of 5 kV. Before observation, the samples were sputtered with platinum layers for 30 s to enhance their electrical conductivity. The surface chemistry of samples was investigated by a Fourier transform infrared spectrometer (FTIR S-One, Perkin Elmer, USA) with Omnic software. The element composition was tested by X-ray photoelectron spectroscopy (XPS 250Xi, Thermo Scientific Escalab, USA) using *Al* Kαx-rays ($h\nu = 1486.6$ eV). Survey spectra were recorded with a pass energy of 150 eV. All the binding energies were calibrated by the C1s peak at 284.8 eV of the surface adventitious

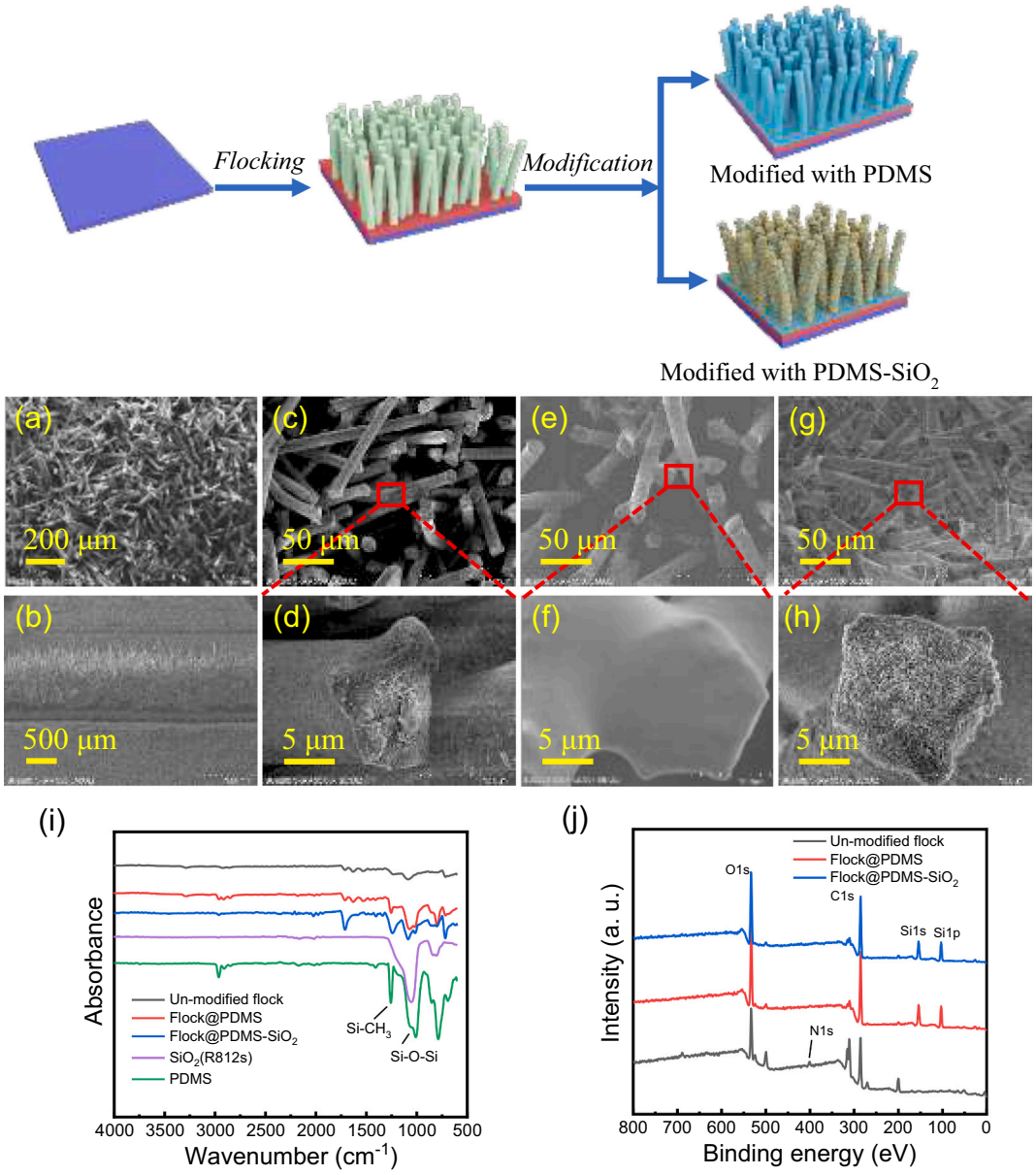

Fig. 2. Fabrication, morphology and surface chemistry of the flocking samples. Top: Schematic illustration showing fabrication of the superhydrophobic flocking samples. Middle: SEM images of the flocking samples (fiber length, 0.6 mm) at different magnifications. (a, b, c, d) Top and side views of the unmodified sample. (e, f) Top views of the sample modified by PDMS and (g, h) the sample by PDMS and nano-SiO2. Bottom: (i) FTIR and (j) XPS spectra of the flocking sample.

carbon.

2.3.2. Surface wettability

The wettability of samples was studied by contact angle measuring apparatus (DSA100, Kruss, Germany) at ambient temperature. Deionized water droplet (4 μL) was carefully dropped onto sample surface and the contact angle was measured. The rolling angle was determined by inclining the sample surface to the angle, at which the water droplet (10 μL) on the surface begun to roll. Each sample was tested 5 times at different positions to minimize experimental errors and the average value was reported.

2.3.3. Mechanical robustness

The mechanical robustness of flocking samples were evaluated by sandpaper abrasion test [35]. A piece of the flocking sample (25 mm × 25 mm) was abraded with a sandpaper (grit No. 240) under an apparent pressure of ~1.6 kPa (using 100 g weight). One sliding cycle includes horizontal slide of 10 cm and normal slide of 10 cm. After every 10-cycle abrasion, the contact angle and rolling angle were measured.

2.3.4. Hydrostatic pressure resistance

The hydrostatic pressure resistance was tested in a sealed transparent pressure tank. The flocking sample was submerged underwater and adjusted to an appropriate angle, at which the silvery reflection zone can be recorded by a digital camera. The silvery reflection zone originated from the air layer trapped on sample. The area of silvery reflection zone reduced with increase in compressed air pressure applied to the sample [36,37] and can be calculated by image processing software (e.g. Image J in this work, see Fig. S2).

2.3.5. Water impact resistance test

The water impact resistance of flocking samples was investigated by water drop test. Individual water droplet (6.3 μL) released from a certain height impacted on the sample surface at different speeds. This process

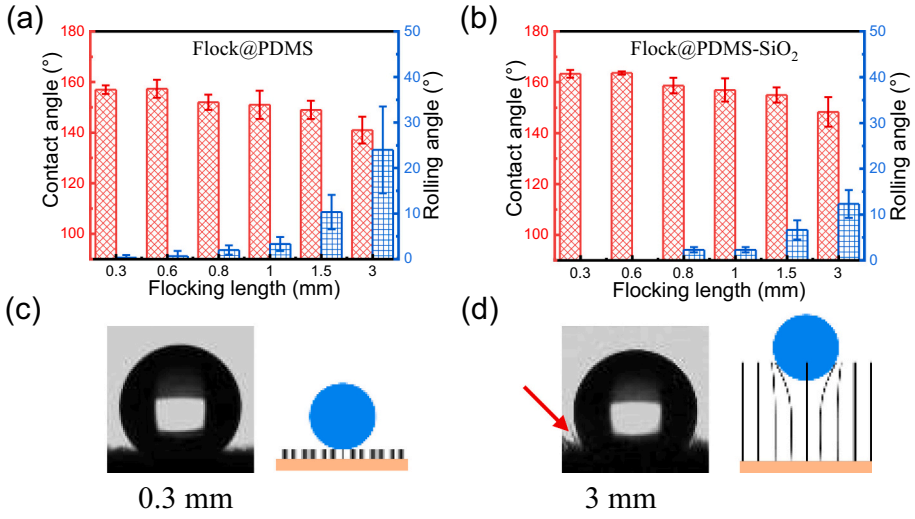

Fig. 3. Wettability of flocking samples with different flocking length. Contact angle (CA) and rolling angle (RA) of the samples modified by (a) PDMS and (b) PDMS-SiO_2. (c, d) Optical photographs showing the water droplets on the PDMS modified samples with flocking length of 0.3 mm and 3.0 mm, respectively. The bending of a flock is indicated by the red arrow in panel d, the related schematic diagrams are shown on the right side. (For interpretation of the references to colour in this figure legend, the reader is referred to the web version of this article.)

was recorded using a Phantom V7.1 colour high-speed camera (Vision Research AMETEK Inc., USA, 3000 frame/s) [38].

2.3.6. Drag-reduction test

For a laminar flow system, the liquid-solid friction can be measured by a rheometer [39–41]. Here, the friction of flocking sample with liquid was explored by a plate-plate rheometer (Thermo Scientific Haake Mars III rheometer, Germany) at room temperature. Fig. S3 presents the schematic diagram of this test. Glycerol-water mixture (50 wt%) served as the testing liquid to reduce experimental error [40]. The plate was 35 mm in diameter. The lower plate was fixed and the upper plate can rotate at certain shear rate. The distance between two plates was kept at 1 mm. As the current shear rate from 40 to 120 s^{-1}, the Reynolds number, R_e, was calculated to be from 156 to 470, which was <2000, verifying the laminar flow of the system ($Re = \frac{\rho R^2 \omega}{\eta}$, where ρ and η are the density and dynamic viscosity of liquid, R is the plate radius, ω is linear velocity). At first test, the steel lower plate (i.e. the flat surface without application of any coatings) was used for measurement, and the torque generated by the testing liquid at various shear rate, M_{flat}, was recorded as control; then the lower plate was covered with the flocking sample, the torque generated at the same shear rate range was measured again, written as M_{flock}. The "drag-reduction level", DR, can be defined according to the equation [12,40,42–44]:

$$DR = \frac{M_{flat} - M_{flock}}{M_{flat}} \quad (1)$$

3. Results and discussion

3.1. Surface properties

Fig. 2 (Top) shows the general fabrication process of the samples. An aluminum foil is coated with the uncured epoxy adhesive, electroflocked with short nylon fibers under high electric voltage (Fig. S1), and subsequently cured at high temperature. After thermal cure, the flocking samples are surface-modified with PDMS (Flock@PDMS) or PDMS containing hydrophobic nano-SiO_2 (Flock@PDMS-SiO_2). And the resulting samples are obtained.

The SEM micrographs in Fig. 2 (Middle) show the typical morphologies of the flocking samples. The flocking samples have relatively good orientation, normal to substrate, forming hairy microstructures (Fig. 2a and b). Mimicking the creatures which is able to secrete low-surface-energy wax or lipids to their surfaces, we applied PDMS or PDMS-SiO_2 to modify the samples in order to offer the samples superhydrophobicity. Compared with the un-modified flocking surface (Fig. 2c and d), a thin and smooth layer of PDMS can be recognized on the fibers (Fig. 2e and f). In the case of sample modified by PDMS-SiO_2, nanoparticle layers can be found (Fig. 2g and h).

The FTIR spectra of the flocking surfaces are shown in Fig. 2i. Compared with the unmodified flocking surface, the characteristic peaks of Si-CH_3 at 1266 cm^{-1} and Si—O—Si at 1025 cm^{-1} appear on the flocking surfaces modified by PDMS or PDMS-SiO_2, which correspond to the PDMS and/or SiO_2 nanoparticles. Similarly, characteristic peaks of silicon (Si 1s, Si 1p) can be detected from XPS spectra of the modified samples, shown in Fig. 2j. The results of SEM, FTIR and XPS prove that the flocking samples were successfully modified.

The wettability of the samples having different flocking length and surface modification are evaluated by contact angle measurement system and the results are shown in Fig. 3a, b. Before surface modification, the flocking surface is superhydrophilic, water droplets dripping on the surface are absorbed into flocking gaps in seconds due to the hydrophilicity and capillarity of flocks. After surface modification by PDMS (Fig. 3a), the sample becomes unwettable with CA of 148° to163° and RA of 12° to 0°. It is clear that the rough surface and low surface energy can change the wettability of the flocking surfaces dramatically. The flocking length is found to determine the hydrophobic level. At shorter flocking length (≤1 mm), the flock surfaces are superhydrophobic (i.e., CA ≥ 150° and RA ≤ 10°), whereas, with longer flocking length (1.5 and 3 mm), the superhydrophobic properties lose slightly. The samples modified by PDMS-SiO_2 show similar tendency in terms of CA and RA (Fig. 3b) and have better superhydrophobicity than those modified by PDMS only. This should be ascribed to the hierarchical micro/nano structures of these samples (Fig. 2g and f). The alternation of CA and RA with flocking length can be explained below. Due to the electroflocked technique, the surfaces with longer flocks are always sparse than those with shorter flocks. Table 1 compares the flocking density of the different samples when the samples were saturatedly flocked. The flocking density decreases from 967 to 116 fiber/mm^2 as the flocking length increases from 0.3 to 3.0 mm. The longer flocks are assumed to have smaller bending stiffness and can be easier bent under the gravity of water droplets, which may, on one hand, increase the contact surface between flock and droplet, and on the other hand, seizing the water droplets between flocking gap, and consequently limit the rotation of droplets. Fig. 3c and d show the optical photographs of water droplets on sample surfaces. The bending of longer flock under the water droplet can be observed and indicated by a red arrow. The related schematic diagrams are also illustrated.

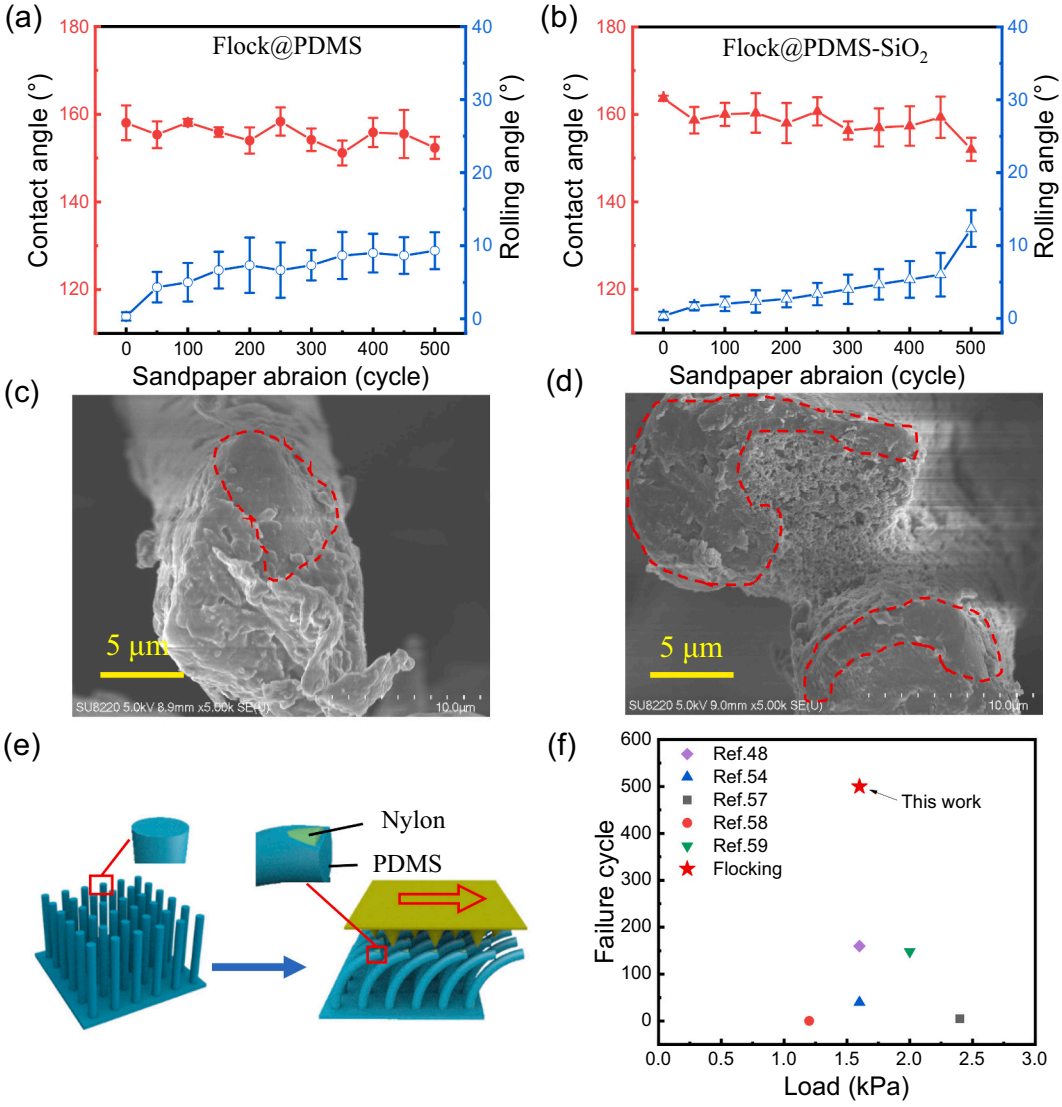

Fig. 4. Wear resistance of the flocking samples. (a, b) The contact angle and rolling angle of Flock@PDMS or Flock@PDMS-SiO_2 samples as functions of abrasion cycle; the samples were subject to 240 mesh sandpaper abrasion under an apparent pressure of 1.6 kPa. (c, d) SEM images of worn surfaces of Flock@PDMS and Flock@PDMS-SiO_2 samples after 200 cycle sandpaper abrasion. (e) Schematic illustration of the self-adaptive deformation of flocks on wearing. (f) Comparison of superhydrophobicity failure cycle of various superhydrophobic materials, which were tested at similar conditions [48,54,57–59].

3.2. Wear resistance

Poor wear resistance is one of the main issues that limit the real applications of the superhydrophobic surfaces [38,45,46]. Fig. 4 presents the wear resistance of the modified flocking samples tested by sandpaper abrasion method. For all flocking samples, their contact angles change little and the rolling angles increase slightly with increased abrasion cycle (Fig. 4a and b). The Flock@PDMS-SiO_2 samples seems better than Flock@PDMS sample, when subject to the same level abrasion. The Flock@PDMS-SiO_2 samples can withstand >500 cycles of sandpaper abrasion at the apparent pressure of ~1.6 kPa, reaching the higher level among the superhydrophobic surfaces tested at similar conditions [45,47–52].

Fig. 4c and d present the SEM worn surfaces of samples after 200 cycles of sandpaper abrasion. Both the top and side of flocks are observed to be worn, as highlighted by the red dashed lines, but the worn level is not serious. The good wear resistance of the flocking samples could be attributed to the high strength and resilience of the micro nylon fiber itself, which can protect the flocking's hydrophobic layer and nanostructures effectively. Unlike some rigid superhydrophobic surfaces [38,53–56], the resilient nylon fibers can swing, bend and orient along abrasion direction (self-adaptive) to avoid "hard to hard" abrasion. Once unloading, the fibers can return to their original state quickly. This feature is illustrated in Fig. 4e. We roughly compare the superhydrophobicity failure cycles of various superhydrophobic materials, which were tested at similar sandpaper abrasion conditions; our flocking sample is the most wear-resistant.

3.3. The stability of air layer

The superhydrophobic surfaces have been reported to have excellent drag-reduction properties under water owing to their unique nano- and micro-structures, which can retain a large amount of air, which can reduce the liquid-solid contact area and thus decreasing the friction between water and the surface effectively. However, sustaining the stability of the air layer under water is still a big issue [21]. The air layer of a common superhydrophobic surface (composed of nano- and micro-sized particles) is very vulnerable to the working conditions, such as the water flow, water pressure, and water impact or intensive vibration [21,36,60]. Under such conditions, the air layer is easily destroyed, the

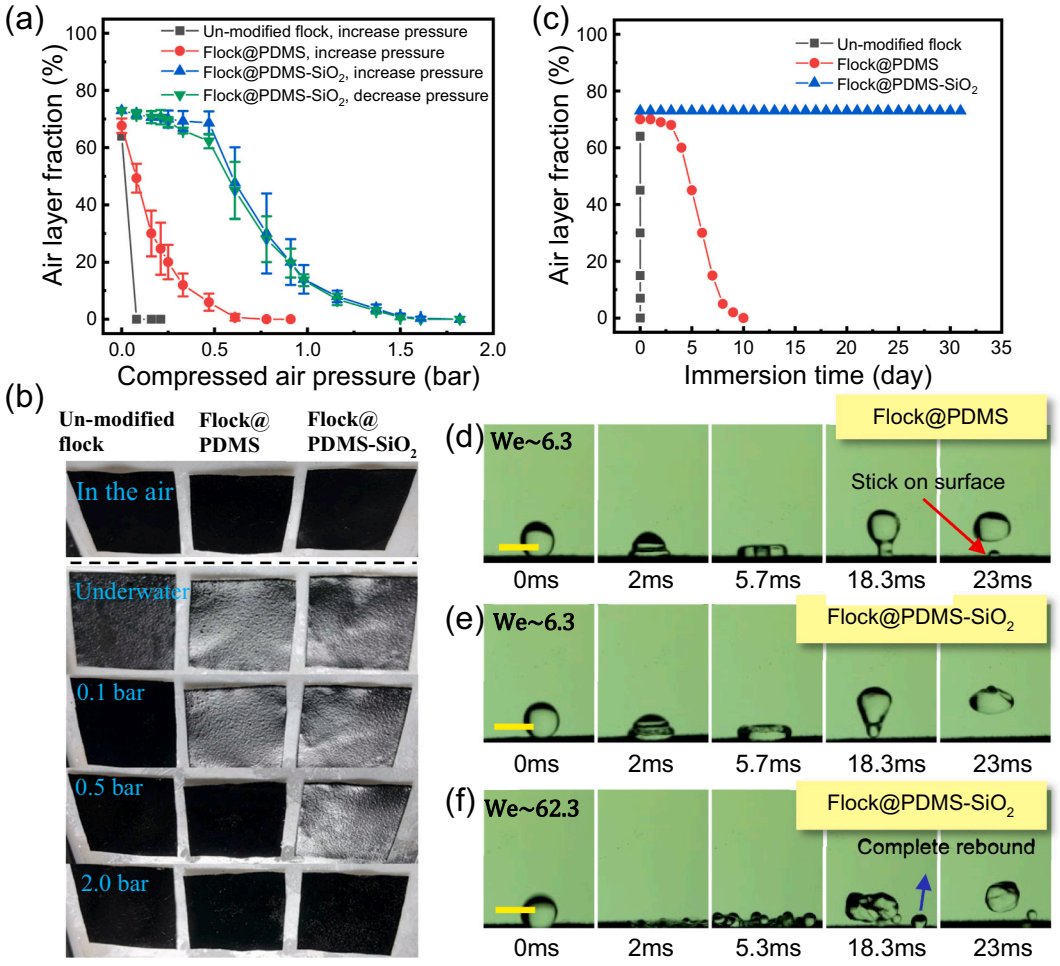

Fig. 5. The stability of air layer of flocking samples. (a) Air layer fraction of flocking samples tested under different compressed air pressures. (b) The related photos of (a). (c) Air layer fraction of flocking samples over immersion time, tested at 1 atmospheric pressure. The droplet impact resistance of flocking samples. (d-f) Photos showing water droplet impacting on (d) Flock@PDMS at *We*~6.3, the water droplet breaks into several small parts and a tiny droplet is stuck on the sample surface (red arrow); (e) Flock@PDMS-SiO_2 at *We*~6.3, the water droplet does not break; and (f) Flock@PDMS-SiO_2 at *We*~62.3, the water droplet breaks but does not stick on the surface. The scale bar is 2.5 mm. (For interpretation of the references to colour in this figure legend, the reader is referred to the web version of this article.)

nano- and micro-structures are wetted by water completely, and subsequently the drag-reduction effect is lost. The stability of the air layer could be evaluated by hydrostatic pressure resistance and water impact resistance tests in laboratory [22,36,60–63].

Here, flocking samples with fiber length of 0.6 mm are selected to investigate their hydrostatic pressure resistance. The unmodified flocking sample is also tested for comparison. Fig. 5a-c shows the results of the samples immersed in water. The experimental photos are shown in Fig. 5b and the area of air layer on samples at different compressed air pressures is estimated by Image J (Section 2.3.4). As shown in Fig. 5a and b, the silvery air layers can be observed on all samples at the very beginning of water immersion. With increase in compressed air pressure, the area of air layer decreases obviously because the enhanced pressure makes water infiltrate into the space between flocks easily. The critical air pressures at which the air layer almost completely disappears are 0.15, 0.6 and 2 bar, corresponding to the un-modified flock, Flock@PDMS and Flock@PDMS-SiO_2 samples, respectively.

Interestingly, for Flock@PDMS-SiO_2, its air layer can be restored once the air pressure releases. This could be ascribed to the fact that the Flock@PDMS-SiO_2 sample has hierarchical nano-micro structures, which offer higher critical capillary pressure [64–67]. The critical capillary pressure of the nanostructure is much greater than the micro-pillar flocks. Under higher air pressure, the air layer may be compressed and trapped in nano-structures rather than replaced by water (Fig. S4), therefore, the silver reflector disappears. However, the sample still maintains non-wetted state, once the pressure is released, the air layer can restore.

Fig. 5c presents the stability of air layer of the samples with immersion time under water at 1 atmospheric pressure. Clearly, the Flock@PDMS-SiO_2 sample exhibits much better air layer stability than others, it can keep the air layer for as long as one month, whereas air layers disappear in a few days and within tens of minutes for Flock@PDMS and unmodified sample, respectively. The Flock@PDMS-SiO_2 sample remains superhydrophobicity with CA of 162 ± 3° and RA of 0–3°, as the sample was taken out of water.

Fig. 5d-f presents the droplet impact resistance of the superhydrophobic flocking samples. At the Weber number of ~6.3, for the sample Flock@PDMS, the water droplet is observed to break into several small parts, and some parts are stuck on the sample surface, as indicated by a red arrow in Fig. 5d. Comparatively, no impalement was observed in the case of sample Flock@PDMS-SiO_2 (Fig. 5e) at the same Weber number of 6.3. The latter sample can withstand the droplet impact at higher Weber number of 62.3. At such a condition, all broken parts are observed to rebound from sample surface without obvious sticking (Fig. 5f).

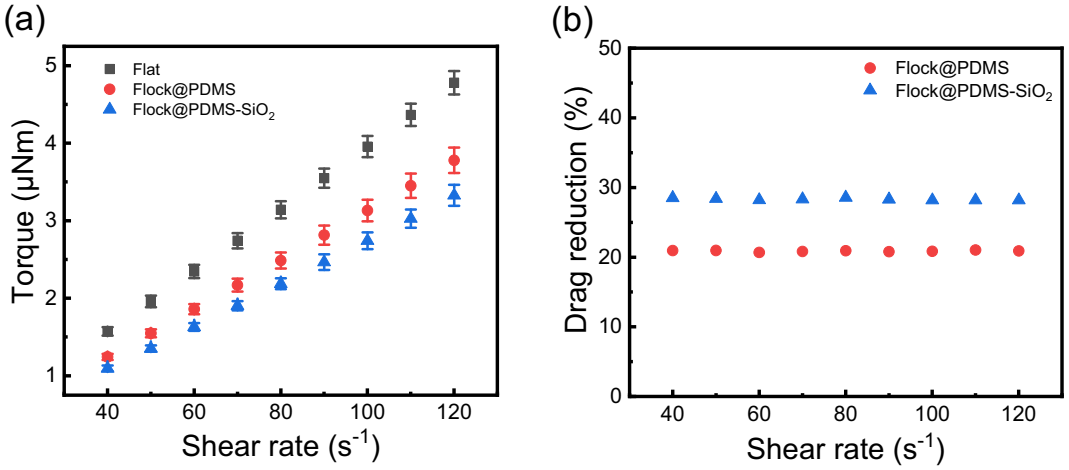

Fig. 6. Drag-reduction properties of samples tested in shear rate of 40–120 s^{-1} using a flat rheometer. (a) Tested torque. (b) Drag-reduction level.

3.4. Drag-reduction level

The drag-reduction level (DR) of flocking samples is estimated by a plate rheometer as mention in Section 2.3.6. Fig. 6a presents the torques tested in shear rate of 40–120 s^{-1} are almost linearly correlated with increasing the shear rate for all samples. The torques for the surface-modified flocking surfaces are obviously lower than that of flat steel plate. Therefore, the DR is calculated according to Eq. (1) and shown in Fig. 6b. DR does not decay in the testing shear rate. The DR value is 21 % and 28 % for the Flock@PDMS and Flock@PDMS-SiO_2, exhibiting good drag-reduction property.

4. Conclusion

Inspired by creature, we fabricated hairy surfaces using electrostatic flocking technique and subsequent surface modification. These samples, owing to their unique micro- and nano-structures, had the excellent superhydrophobic properties with water contact angle of 163° and rolling angle of ~0°. Owing to self-adaptive deformation of flocks, the samples withstood >500 cycles of sandpaper abrasion at the apparent pressure of ~1.6 kPa without significant loss of their superhydrophobic performance. They can retain their air layers under water when pressured to 2 bar using compressed air or keep the air layers for as long as one month at normal atmosphere. Also, the samples withstood the water drop impact with Weber number of ~62.3. The samples did show effective drag-reduction with the maximum drag-reduction efficiency of 28 %. This hairy superhydrophobic surfaces seem very promising for drag-reduction applications.

CRediT authorship contribution statement

Liangpei Zhang: Conceptualization, Methodology, Investigation, Visualization, Writing – original draft, Writing – review & editing. **Zhaohui Huang:** Funding acquisition, Supervision. **Wenfu Cai:** Methodology, Investigation. **Xiao Xue:** Methodology, Investigation. **Xin Min:** Methodology, Investigation. **Hui Zhang:** Conceptualization, Methodology, Writing – review & editing, Supervision. **Zhong Zhang:** Project administration, Funding acquisition, Resources.

Declaration of competing interest

All authors disclosed no relevant relationships.

Data availability

No data was used for the research described in the article.

Acknowledgements

This work was financially supported by Regional Key Projects of Science and Technology Service Network Program of Chinese Academy of Sciences (KFJ-STS-QYZD-121) and The Austrian-Chinese Cooperative Research and Development Projects (GJHZ2043), Chinese Academy of Sciences.

References

[1] In 2020, 90, 000 seaborne ships around the world will consume 350 million metric tons of fuel annually, in: International Ship & Offshore Network, 2019. http://ishipoffshore.com/html/7/2019-08-14/9782.htm.
[2] B. Dean, B. Bhushan, Shark-skin surfaces for fluid-drag reduction in turbulent flow: a review, Philos. Trans. R. Soc., A 368 (2010) 4775–4806, https://doi.org/10.1098/rsta.2010.0201.
[3] X. Pu, G. Li, H. Huang, Preparation, anti-biofouling and drag-reduction properties of a biomimetic shark skin surface, Biol. Open 5 (2016) (2016) 389–396, https://doi.org/10.1242/bio.016899.
[4] Y.C. Jung, B. Bhushan, Biomimetic structures for fluid drag reduction in laminar and turbulent flows, J. Phys.: Condens. Matter 22 (2010) 035104, https://doi.org/10.1088/0953-8984/22/3/035104.
[5] S. Park, J.M. Wallace, Flow alteration and drag reduction by riblets in a turbulent boundary layer, AIAA J. 32 (1994) (1994) 31–38, https://doi.org/10.2514/3.11947.
[6] D.W. Bechert, M. Bruse, W. Hage, Experiments with three-dimensional riblets as an idealized model of shark skin, Exp. Fluids 28 (2000) (2000) 403–412, https://doi.org/10.1007/s003480050400.
[7] H. Zhao, J.Z. Wu, J.S. Luo, Turbulent drag reduction by traveling wave of flexible wall, Fluid Dyn. Res. 34 (2004) (2004) 175–198, https://doi.org/10.1016/j.fluiddyn.2003.11.001.
[8] D. Saranadhi, D. Chen, J.A. Kleingartner, S. Srinivasan, R.E. Cohen, G.H. McKinley, Sustained drag reduction in a turbulent flow using a low-temperature leidenfrost surface, Sci. Adv. 2 (2016) (2016), e1600686, https://doi.org/10.1126/sciadv.1600686.
[9] I.U. Vakarelski, J.D. Berry, D.Y. Chan, S.T. Thoroddsen, Leidenfrost vapor layers reduce drag without the crisis in high viscosity liquids, Phys. Rev. Lett. 117 (2016) (2016), 114503, https://doi.org/10.1103/PhysRevLett.117.114503.
[10] I.U. Vakarelski, J.O. Marston, D.Y.C. Chan, S.T. Thoroddsen, Drag reduction by leidenfrost vapor layers, Phys. Rev. Lett. 106 (2011) (2011), 214501, https://doi.org/10.1103/PhysRevLett.106.214501.
[11] K.M.Tanvir Ahmmed, A.M. Kietzig, Drag reduction on laser-patterned hierarchical superhydrophobic surfaces, Soft Matter 12 (2016) 4912–4922, https://doi.org/10.1039/c6sm00436a.
[12] H. Xu, C.R. Crick, R.J. Poole, Evaluating the resilience of superhydrophobic materials using the slip-length concept, J. Mater. Chem. A 6 (2018) (2018) 4458–4465, https://doi.org/10.1039/c7ta10510j.
[13] Y. Tuo, W. Chen, H. Zhang, P. Li, X. Liu, One-step hydrothermal method to fabricate drag reduction superhydrophobic surface on aluminum foil, Appl. Surf. Sci. 446 (2018) (2018) 230–235, https://doi.org/10.1016/j.apsusc.2018.01.046.

[14] E. Taghvaei, A. Moosavi, A. Nouri-Borujerdi, M.A. Daeian, S. Vafaeinejad, Superhydrophobic surfaces with a dual-layer micro- and nanoparticle coating for drag reduction, Energy 125 (2017) (2017) 1–10, https://doi.org/10.1016/j.energy.2017.02.117.
[15] E. Liu, L. Li, G. Wang, Z. Zeng, W. Zhao, Q. Xue, Drag reduction through self-texturing compliant bionic materials, Sci. Rep. 7 (2017) (2017) 40038, https://doi.org/10.1038/srep40038.
[16] C. Lee, C. Choi, C. Kim, Superhydrophobic drag reduction in laminar flows: a critical review, Exp. Fluids 57 (2016) (2016) 176, https://doi.org/10.1007/s00348-016-2264-z.
[17] D. Song, R.J. Daniello, J.P. Rothstein, Drag reduction using superhydrophobic sanded teflon surfaces, Exp. Fluids 55 (2014) (2014) 1783, https://doi.org/10.1007/s00348-014-1783-8.
[18] H. Dong, M. Cheng, Y. Zhang, H. Wei, F. Shi, Extraordinary drag-reducing effect of a superhydrophobic coating on a macroscopic model ship at high speed, J. Mater. Chem. A 1 (2013) (2013) 5886, https://doi.org/10.1039/c3ta10225d.
[19] C. Lee, C. Kim, Underwater restoration and retention of gases on superhydrophobic surfaces for drag reduction, Phys. Rev. Lett. 106 (2011) (2011), 014502, https://doi.org/10.1103/PhysRevLett.106.014502.
[20] C. Lee, C.J.J.C. Kim, Influence of surface hierarchy of superhydrophobic surfaces on liquid slip, Langmuir 27 (2011) (2011) 4243–4248, https://doi.org/10.1021/la104368v.
[21] M.N. Kavalenka, F. Vullers, S. Lischker, C. Zeiger, A. Hopf, M. Rohrig, B.E. Rapp, M. Worgull, H. Holscher, Bioinspired air-retaining nanofur for drag reduction, ACS Appl. Mater. Interfaces 7 (2015) (2015) 10651–10655, https://doi.org/10.1021/acsami.5b01772.
[22] P. Papadopoulos, L. Mammen, X. Deng, D. Vollmer, H.J. Butt, How superhydrophobicity breaks down, Proc. Natl. Acad. Sci. U. S. A. 110 (2013) (2013) 3254–3258, https://doi.org/10.1073/pnas.1218673110.
[23] P. Ditschekuru, E.S. Schneider, J. Melskotte, M. Brede, A. Leder, W. Barthlott, Superhydrophobic surfaces of the water bug Notonecta glauca: a model for friction reduction and air retention, Beilstein J. Nanotechnol. 2 (2011) (2011) 137–144, https://doi.org/10.3762/bjnano.2.17.
[24] X. Gao, L. Jiang, Biophysics: water-repellent legs of water striders, Nature 432 (2004) (2004) 36, https://doi.org/10.1038/432036a.
[25] T. Darmanin, F. Guittard, Superhydrophobic and superoleophobic properties in nature, Mater. Today 18 (2015) (2015) 273–285, https://doi.org/10.1016/j.mattod.2015.01.001.
[26] J.W.M. Bush, D.L. Hu, M. Prakash, The integument of water-walking arthropods: form and function, Adv. Insect Physiol. 34 (2007) (2007) 117–192, https://doi.org/10.1016/S0065-2806(07)34003-4.
[27] D.L. Hu, J.W. Bush, Meniscus-climbing insects, Nature 437 (2005) (2005) 733–736, https://doi.org/10.1038/nature03995.
[28] W. Barthlott, T. Schimmel, S. Wiersch, K. Koch, M. Brede, M. Barczewski, S. Walheim, A. Weis, A. Kaltenmaier, A. Leder, H. Bohn, Superhydrophobic coatings: the salvinia paradox: superhydrophobic surfaces with hydrophilic pins for air retention under water, Adv. Mater. 22 (2010) (2010) 2325–2328, https://doi.org/10.1002/adma.201090075.
[29] X. Li, J. Yang, K. Lv, P. Papadopoulos, J. Sun, D. Wang, Y. Zhao, L. Chen, D. Wang, Z. Wang, X. Deng, Salvinia-like slippery surface with stable and mobile water/air contact line, Natl. Sci. Rev. 8 (2021), nwaa153, https://doi.org/10.1093/nsr/nwaa153.
[30] Y. Zheng, X. Zhou, Z. Xing, T. Tu, Fabrication of a superhydrophobic surface with underwater air-retaining properties by electrostatic flocking, RSC Adv. 8 (2018) (2018) 10719–10726, https://doi.org/10.1039/c7ra13262j.
[31] Y. Liu, X. Chen, J.H. Xin, Hydrophobic duck feathers and their simulation on textile substrates for water repellent treatment, Bioinspiration Biomimetics 3 (2008) (2008), 046007, https://doi.org/10.1088/1748-3182/3/4/046007.
[32] S. Wang, Z. Yang, G. Gong, J. Wang, J. Wu, S. Yang, L. Jiang, Icephobicity of penguins spheniscus humboldti and an artificial replica of penguin feather with air-infused hierarchical rough structures, J. Phys. Chem. C 120 (2016) (2016) 15923–15929, https://doi.org/10.1021/acs.jpcc.5b12298.
[33] Y. Xiang, S. Huang, T.-Y. Huang, A. Dong, D. Cao, H. Li, Y. Xue, P. Lv, H. Duan, Superrepellency of underwater hierarchical structures on salvinia leaf, Proc. Natl. Acad. Sci. U. S. A. 117 (2020) (2020) 2282–2287, https://doi.org/10.1073/pnas.1900015117.
[34] J.W.M. Bush, D.L. Hu, M. Prakash, The integument of water-walking arthropods: form and function, Adv. Insect Physiol. 34 (2007) (2017) 117–192, https://doi.org/10.1016/S0065-2806(07)34003-4.
[35] M. Im, H. Im, J.-H. Lee, J.-B. Yoon, Y.-K. Choi, A robust superhydrophobic and superoleophobic surface with inverse-trapezoidal microstructures on a large transparent flexible substrate, Soft Matter 6 (2010) (2010) 1401–1404, https://doi.org/10.1039/b925970h.
[36] M.S. Bobji, S.V. Kumar, A. Asthana, R.N. Govardhan, Underwater sustainability of the "Cassie" state of wetting, Langmuir 25 (2009) (2009) 12120–12126, https://doi.org/10.1021/la902679c.
[37] L. Lei, H. Li, J. Shi, Y. Chen, Diffraction patterns of a water-submerged superhydrophobic grating under pressure, Langmuir 26 (2009) (2009) 3666–3669, https://doi.org/10.1021/la903150h.
[38] C. Peng, Z. Chen, M.K. Tiwari, All-organic superhydrophobic coatings with mechanochemical robustness and liquid impalement resistance, Nat. Mater. 17 (2018) (2018) 355–360, https://doi.org/10.1038/s41563-018-0044-2.
[39] C. Choi, C. Kim, Large slip of aqueous liquid flow over a nanoengineered superhydrophobic surface, Phys. Rev. Lett. 96 (2006) (2006), 066001, https://doi.org/10.1103/PhysRevLett.96.066001.
[40] S. Srinivasan, W. Choi, K.-C. Park, S.S. Chhatre, R.E. Cohen, G.H. McKinley, Drag reduction for viscous laminar flow on spray-coated non-wetting surfaces, Soft Matter 9 (2013) (2013) 5691–5702, https://doi.org/10.1039/c3sm50445j.
[41] J.P. Rothstein, Slip on superhydrophobic surfaces, Annu. Rev. Fluid Mech. 42 (2010) (2010) 89–109, https://doi.org/10.1146/annurev-fluid-121108-145558.
[42] C. Lee, C. Choi, C.C. Kim, Structured surfaces for a giant liquid slip, Phys. Rev. Lett. 101 (2008) (2008), 064501, https://doi.org/10.1103/PhysRevLett.101.064501.
[43] Z. Ming, L. Jian, W. Chunxia, Z. Xiaokang, C. Lan, Fluid drag reduction on superhydrophobic surfaces coated with carbon nanotube forests (CNTs), Soft Matter 7 (2011) (2011) 4391–4396, https://doi.org/10.1039/c0sm01426e.
[44] S. Srinivasan, J.A. Kleingartner, J.B. Gilbert, R.E. Cohen, A.J. Milne, G. H. McKinley, Sustainable drag reduction in turbulent Taylor-Couette flows by depositing sprayable superhydrophobic surfaces, Phys. Rev. Lett. 114 (2015) (2015), 014501, https://doi.org/10.1103/PhysRevLett.114.014501.
[45] D. Wang, Q. Sun, M.J. Hokkanen, C. Zhang, F.-Y. Lin, Q. Liu, S.-P. Zhu, T. Zhou, Q. Chang, B. He, Q. Zhou, L. Chen, Z. Wang, R.H.A. Ras, X. Deng, Design of robust superhydrophobic surfaces, Nature 582 (2020) (2020) 55–59, https://doi.org/10.1038/s41586-020-2331-8.
[46] X. Tian, T. Verho, R.H.A. Ras, Surface wearMoving superhydrophobic surfaces toward real-world applications, Science 352 (2016) (2016) 142–143, https://doi.org/10.1126/science.aaf2073.
[47] H. Zhou, H. Wang, H. Niu, A. Gestos, X. Wang, T. Lin, Fluoroalkyl silane modified silicone rubber/nanoparticle composite: a super durable, robust superhydrophobic fabric coating, Adv. Mater. 24 (2012) (2012) 2409–2412, https://doi.org/10.1002/adma.201200184.
[48] Y. Lu, S. Sathasivam, J. Song, C.R. Crick, C.J. Carmalt, I.P. Parkin, Repellent materials. Robust self-cleaning surfaces that function when exposed to either air or oil, Science 347 (2015) 1132–1135, https://doi.org/10.1126/science.aaa0946.
[49] Y. Li, B. Ge, X. Men, Z. Zhang, Q. Xue, A facile and fast approach to mechanically stable and rapid self-healing waterproof fabrics, Compos. Sci. Technol. 125 (2016) (2016) 55–61, https://doi.org/10.1016/j.compscitech.2016.01.021.
[50] J. Zhi, L.Z. Zhang, Durable superhydrophobic surfaces made by intensely connecting a bipolar top layer to the substrate with a middle connecting layer, Sci. Rep. 7 (2017) (2017) 9946, https://doi.org/10.1038/s41598-017-10030-9.
[51] F.J. Wang, S. Lei, J.F. Ou, M.S. Xue, W. Li, Superhydrophobic surfaces with excellent mechanical durability and easy repairability, Appl. Surf. Sci. 276 (2013) (2013) 397–400, https://doi.org/10.1016/j.apsusc.2013.03.104.
[52] A. Davis, S. Surdo, G. Caputo, I.S. Bayer, A. Athanassiou, Environmentally benign production of stretchable and robust superhydrophobic silicone monoliths, ACS Appl. Mater. Interfaces 10 (2018) (2018) 2907–2917, https://doi.org/10.1021/acsami.7b15088.
[53] N. Wang, D. Xiong, Y. Deng, Y. Shi, K. Wang, Mechanically robust superhydrophobic steel surface with anti-icing, UV-durability, and corrosion resistance properties, ACS Appl. Mater. Interfaces 7 (2015) (2015) 6260–6272, https://doi.org/10.1021/acsami.5b00558.
[54] J. Han, M. Cai, Y. Lin, W. Liu, X. Luo, H. Zhang, K. Wang, M. Zhong, Comprehensively durable superhydrophobic metallic hierarchical surfaces via tunable micro-cone design to protect functional nanostructures, RSC Adv. 8 (2018) (2018) 6733–6744, https://doi.org/10.1039/c7ra13496g.
[55] J. Lomga, P. Varshney, D. Nanda, M. Satapathy, S.S. Mohapatra, A. Kumar, Fabrication of durable and regenerable superhydrophobic coatings with excellent self-cleaning and anti-fogging properties for aluminium surfaces, J. Alloys Compd. 702 (2017) (2017) 161–170, https://doi.org/10.1016/j.jallcom.2017.01.243.
[56] T. Maitra, C. Antonini, M.A.D. Mauer, C. Stamatopoulos, M.K. Tiwari, D. Poulikakos, Hierarchically nanotextured surfaces maintaining superhydrophobicity under severely adverse conditions, Nanoscale 6 (2014) (2014) 8710–8719, https://doi.org/10.1039/c4nr01368a.
[57] F. Su, K. Yao, Facile fabrication of superhydrophobic surface with excellent mechanical abrasion and corrosion resistance on copper substrate by a novel method, ACS Appl. Mater. Interfaces 6 (2014) 8762–8770, https://doi.org/10.1021/am501539b.
[58] N. Wang, D. Xiong, Y. Deng, Y. Shi, K. Wang, Mechanically robust superhydrophobic steel surface with anti-icing, UV-durability, and corrosion resistance properties, ACS Appl. Mater. Interfaces 7 (2015) 6260–6272, https://doi.org/10.1021/acsami.5b00558.
[59] X. Chen, Y. Gong, D. Li, H. Li, Robust and easy-repairable superhydrophobic surfaces with multiple length-scale topography constructed by thermal spray route, Colloids Surf. A Physicochem. Eng. Asp. 492 (2016) 19–25, https://doi.org/10.1016/j.colsurfa.2015.12.017.
[60] X. Sheng, J. Zhang, Air layer on superhydrophobic surface underwater, Colloids Surf., A 377 (2011) 374–378, https://doi.org/10.1016/j.colsurfa.2011.01.033.
[61] B. Liu, F.F. Lange, Pressure induced transition between superhydrophobic states: configuration diagrams and effect of surface feature size, J. Colloid Interface Sci. 298 (2006) (2006) 899–909, https://doi.org/10.1016/j.jcis.2006.01.025.
[62] E. Huovinen, J. Hirvi, M. Suvanto, T.A. Pakkanen, Micro-micro hierarchy replacing micro-nano hierarchy: a precisely controlled way to produce wear-resistant superhydrophobic polymer surfaces, Langmuir 28 (2012) (2012) 14747–14755, https://doi.org/10.1021/la303358h.
[63] H. Teisala, F. Geyer, J. Haapanen, P. Juuti, J.M. Makela, D. Vollmer, H.J. Butt, Ultrafast processing of hierarchical nanotexture for a transparent superamphiphobic coating with extremely low roll-off angle and high impalement pressure, Adv. Mater. 30 (2018) (2018), e1706529, https://doi.org/10.1002/adma.201706529.
[64] M. McCarthy, K. Gerasopoulos, R. Enright, J. Culver, R. Ghodssi, E. Wang, Biotemplated hierarchical surfaces and the role of dual length scales on the

repellency of impacting droplets, Appl. Phys. Lett. 100 (2012) (2012), 263701, https://doi.org/10.1063/1.4729935.
[65] T. Maitra, M.K. Tiwari, C. Antonini, P. Schoch, S. Jung, P. Eberle, D. Poulikakos, On the nanoengineering of superhydrophobic and impalement resistant surface textures below the freezing temperature, Nano Lett. 14 (2014) (2014) 172–182, https://doi.org/10.1021/nl4037092.
[66] D. Bartolo, F. Bouamrirene, E. Verneuil, A. Buguin, P. Silberzan, S. Moulinet, Bouncing or sticky droplets impalement transitions on superhydrophobic micropatterned surfaces, Europhys. Lett. 74 (2006) (2006) 299–305, https://doi.org/10.1209/epl/i2005-10522-3.
[67] P. Brunet, F. Lapierre, Thomy, Y. Coffinier, R. Boukherroub, Extreme resistance of superhydrophobic surfaces to impalement: reversible electrowetting related to the impacting/bouncing drop test, Langmuir 24 (2008) 11203–11208, https://doi.org/10.1021/la801268v.